

# Rapid and Inexpensive Inertia Tensor Estimation from a Single Object Throw

Till M. Blaha\*, Mike M. Kuijper\*, Radu Pop, Ewoud J.J. Smeur

**Abstract**—The inertia tensor is an important parameter in many engineering fields, but measuring it can be cumbersome and involve multiple experiments or accurate and expensive equipment. We propose a method to measure the moment of inertia tensor of a rigid body from a single spinning throw, by attaching a small and inexpensive stand-alone measurement device consisting of a gyroscope, accelerometer and a reaction wheel. The method includes a compensation for the increase of moment of inertia due to adding the measurement device to the body, and additionally obtains the location of the centre of gravity of the body as an intermediate result. Experiments performed with known rigid bodies show that the mean accuracy is around 2%.

**Index Terms**—Calibration and Identification, Dynamics

## I. INTRODUCTION

IN numerous applications, the mass properties of a rigid body are essential quantities required for computing its dynamic behaviour. This applies to various fields, from physics to engineering and robotics. For example, it is required for accurate simulation and control of satellites, robots, and (flying) vehicles. While the mass of an object can often be easily and directly measured, the inertia tensor governing the rotational motion cannot.

When the mass distribution of an object is known, e.g. from a Computer Aided Design (CAD) program, then its inertia can be calculated in a straightforward fashion. However, the amount of parts that make up a rigid body can be very high, and not every small part may be accounted for. Moreover, manufacturing imperfections may lead to deviations from the predicted inertia tensor in practice. Finally, 3D models with accurate densities may not be available for all objects of interest. In these cases, the inertia of an object has to be determined experimentally.

The most straightforward method is to measure the inertia tensor robotically by restricting the object to rotate around one axis and applying a known torque in this axis. From the angular acceleration, the inertia about this axis can be determined [1]. For this method the object needs to be accurately mounted to the robot, potentially requiring some adapter. The accuracy of the method will largely depend on the

This work has been submitted to the IEEE for possible publication. Copyright may be transferred without notice, after which this version may no longer be accessible.

<sup>1</sup>The authors are with the Faculty of Aerospace Engineering, Delft University of Technology, The Netherlands.

Till Blaha and Mike Kuijper are co-first authors. Corresponding author: m.m.kuijper@student.tudelft.nl

Digital Object Identifier (DOI): see top of this page.

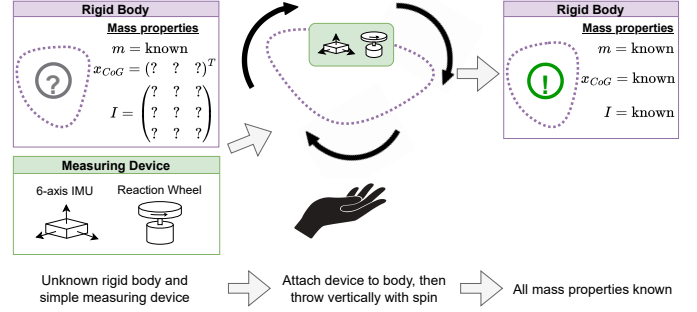


Figure 1: We propose a simple measuring device and procedure to determine inertial properties.

accuracy with which the applied torque is known, necessitating sophisticated hardware. Measurements about multiple axes will have to be performed in order to get the full inertia tensor, and even more measurements if the location of the centre of gravity is unknown as well.

Alternatively, there are multiple pendulum methods, which do not require sophisticated hardware, aside from a means to measure oscillation period (e.g. optically, or using an onboard gyroscope). With the gravitational pendulum method, the object is attached to an axis in the horizontal plane, and let free to oscillate. The most accurate results are obtained if the objects' centre of gravity is close to the radius of gyration about that axis [2]. With bifilar pendulum [3], [4] or multifilar pendulum methods, the axis of rotation is the vertical axis [5]. The bifilar pendulum method is a popular low-cost method for vehicles that have gyroscopes onboard. Although these pendulum methods can produce accurate results, they require multiple experiments to obtain the full inertia tensor, and the workload is high due to the requirement of repeatedly suspending the object with wires. In some cases, compensation for aerodynamic effects may be needed [6].

The contribution of this paper is a method to accurately estimate the mass moments of inertia and centre of gravity of a small body in seconds, by only making use of inertial measurements during a single vertical spinning throw of the object. These measurements are obtained from a low-cost device mounted to the object containing a consumer-grade Inertial Measurement Unit (IMU), measuring angular velocities and linear accelerations, together with a reaction wheel capable of delivering a torque.<sup>1</sup>

<sup>1</sup>Data and analysis code: <https://github.com/tudelft/inertiaEstimation>

## II. METHODOLOGY

In the absence of external forces, the rotational behaviour of a rigid body is completely determined by its inertia tensor. This tensor can be represented by

$$(I_{ij}) = \int_{\Omega} (\|\rho\|^2 \delta_{ij} - \rho_i \rho_j) dm, \quad (1)$$

for infinitesimal masses positioned at  $\rho$  from the centre of mass in region  $\Omega$ , where  $\delta_{ij}$  is the Kronecker delta. This is a linear operation, and can thus be summed over different bodies.

Euler's rotation equation states that

$$I\dot{\omega} + \omega \times (I\omega) = M, \quad (2)$$

where  $I$  is the body's inertia tensor,  $\omega$  is the body's angular rotation vector,  $\dot{\omega}$  is the body's angular acceleration, and  $M$  is an external torque. In the absence of an external torque ( $M = 0$ ), this equation is homogeneous, which makes rotation data without external torques ineffective for estimating  $I$ .<sup>2</sup>

Therefore, it is required to introduce a known torque to the system. Figure 2 shows a diagram of a possible implementation that attaches a reaction wheel to provide a torque and an IMU to measure  $\omega$ .

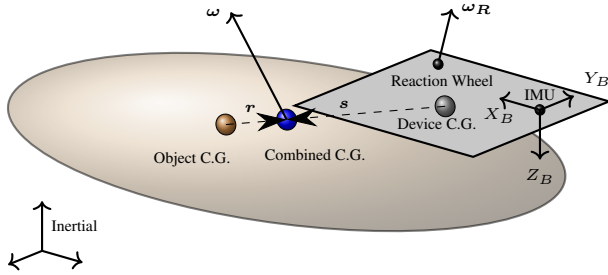


Figure 2: “Object” under test and rigidly attached measuring “Device”. The body-frame  $B$  is defined at the location of the IMU, as shown.

The following sections show how a rigid body with attached reaction wheel, how the equations of motion during free tumbling can be solved for the inertia, and how to calibrate the possibly unknown inertia of the reaction wheel and the measuring device itself.

### A. Deriving rotational equation of motion

In an inertial reference frame, Euler's second law states that external moments change the rotational momentum  $M = (dL/dt)_I$ , where the subscript  $(\square)_I$  denotes that the derivative is taken with respect to the inertial frame. To account for the gyroscopic effects of the reaction wheel, we can write

$$L = I_O \omega + I_R (\omega + \omega_R), \quad (3)$$

where  $I_O$  is the body's inertia tensor excluding rotational inertia of the reaction wheel. The distinction between measurement device and object is made at a later stage.  $\omega$  is

the body's angular velocity vector,  $I_R$  is the reaction wheel's inertia tensor, and  $\omega_R$  is the reaction wheel's angular velocity vector with respect to the body frame.

For the subsequent analysis, it is useful to perform the time-derivative of Equation 3 with respect to a frame fixed to the rigid-body under test, denoted with subscript  $(\square)_B$  in the following. The first equation below is derived in [7]:

$$\begin{aligned} \left(\frac{dL}{dt}\right)_I &= \left(\frac{dL}{dt}\right)_B + \omega \times L \\ M &= \left(\dot{I}_O \omega + I_O \dot{\omega} + \dot{I}_R (\omega + \omega_R) + I_R (\dot{\omega} + \dot{\omega}_R)\right)_B \\ &\quad + \omega \times (I_O \omega + I_R (\omega + \omega_R)) \end{aligned} \quad (4)$$

With respect to the body-fixed frame,  $(\dot{I}_O)_B = 0$ . Furthermore, if we assume that the reaction wheel attached to the body is axisymmetric around its axis of rotation, then  $(\dot{I}_R)_B = 0$  as well since  $I_R$  is then independent of its rotation angle. Dropping the subscript  $B$  for brevity, setting  $M = 0$ , and collecting  $\omega_R$  terms on the right results in the final Equation of Motion:

$$\underbrace{(I_O + I_R)}_I \dot{\omega} + \omega \times \underbrace{(I_O + I_R)}_I \omega = -I_R \dot{\omega}_R - \omega \times (I_R \omega_R). \quad (6)$$

### B. Solving the equation of motion

Equation 6 is linear in the components of  $I$ , and we can represent the left-hand side in the form of  $\zeta_i \theta$ , where  $\zeta_i$  denotes the transformation matrix associated with the  $i$ th datapoint, and  $\theta$  is a vector containing the six unknown components. Let us define

$$I = \begin{bmatrix} I_{xx} & I_{xy} & I_{xz} \\ I_{xy} & I_{yy} & I_{yz} \\ I_{xz} & I_{yz} & I_{zz} \end{bmatrix} \text{ and } \theta = \begin{bmatrix} I_{xx} \\ I_{xy} \\ I_{xz} \\ I_{yy} \\ I_{yz} \\ I_{zz} \end{bmatrix}, \quad (7)$$

and rewrite Equation 6 as

$$\underbrace{\zeta_i \theta}_{I\dot{\omega}_i + \omega_i \times (I\omega_i)} = \underbrace{\mu_i}_{-I_R \dot{\omega}_{Ri} - \omega_i \times (I_R \omega_{Ri})}, \quad (8)$$

where  $\zeta_i$  contains the cross-products of the left-hand side:

$$\zeta_i = \begin{bmatrix} \dot{\omega}_x & \dot{\omega}_y - \omega_z \omega_x & -\omega_z \omega_y & \dot{\omega}_z + \omega_y \omega_x & \omega_y^2 - \omega_z^2 & \omega_y \omega_z \\ \omega_z \omega_x & \dot{\omega}_x + \omega_z \omega_y & \dot{\omega}_y & \omega_z^2 - \omega_x^2 & \dot{\omega}_z - \omega_x \omega_y & -\omega_x \omega_z \\ -\omega_y \omega_x & \omega_x^2 - \omega_y^2 & \omega_x \omega_y & \dot{\omega}_x - \omega_y \omega_z & \dot{\omega}_y + \omega_x \omega_z & \dot{\omega}_z \end{bmatrix}_i. \quad (9)$$

At this point, it is assumed that  $I_R$  is known, so that the right-hand-side  $\mu_i$  can be computed from measurements of the object's rotation rate and the flywheel rotation rate.

Equation 8 is underdetermined, such that multiple observations  $i$  are necessary to solve for  $\theta$ . The least-squares algorithm can be used with an arbitrary number of data points  $i \in 1, \dots, N$  by stacking  $\zeta_1 \dots \zeta_N$  and  $\mu_1 \dots \mu_N$  such that

$$\begin{bmatrix} \zeta_1 \\ \vdots \\ \zeta_N \end{bmatrix} \theta = \begin{bmatrix} \mu_1 \\ \vdots \\ \mu_N \end{bmatrix}. \quad (10)$$

<sup>2</sup>It is possible to extract the ratios between the moments of inertia, but not their absolute values.

1) *Recursive Formulation:* In embedded systems, enough memory to store a long sequence of recorded sensor data may not be available. Equation 10 can be solved recursively by defining

$$A_n = \begin{bmatrix} \zeta_1 \\ \vdots \\ \zeta_n \end{bmatrix} \text{ and } \mathbf{b}_n = \begin{bmatrix} \boldsymbol{\mu}_1 \\ \vdots \\ \boldsymbol{\mu}_n \end{bmatrix}, \quad (11)$$

and then solving the linear least squares problem

$$A_n^T A_n \boldsymbol{\theta} = A_n^T \mathbf{b}_n \Leftrightarrow \left( \sum_{n=1}^N \zeta_n^T \zeta_n \right) \boldsymbol{\theta} = \left( \sum_{n=1}^N \zeta_n^T \boldsymbol{\mu}_n \right), \quad (12)$$

which can be made computationally easier by realising that both  $\zeta_n^T \zeta_n$  and  $\zeta_n^T \boldsymbol{\mu}_n$  are  $6 \times 6$  matrices for  $n \geq 2$ , so that

$$\sum_{n=1}^N \zeta_n^T \zeta_n = \zeta_N^T \zeta_N + \sum_{n=1}^{N-1} \zeta_n^T \zeta_n, \text{ and} \quad (13)$$

$$\sum_{n=1}^N \zeta_n^T \boldsymbol{\mu}_n = \zeta_N^T \boldsymbol{\mu}_N + \sum_{n=1}^{N-1} \zeta_n^T \boldsymbol{\mu}_n. \quad (14)$$

This leads to a constant single-estimate time complexity with respect to  $N$  in the real-time case, as well as significantly reduced memory usage, at the cost of the inability to compute the residuals, which might serve as an error metric.

### C. Correcting for the inertia of the measurement device

The addition of the device to the object has a two-fold effect on the combined mass properties: (1) it moves the centre of mass, and (2) it increases the combined inertia. When recording sensor data of the combined configuration for use with the solution of the previous section, this combined inertia is computed and needs to be corrected, unless the measurement unit's mass is negligible compared to the object under test.

We introduce subscript  $\square_{\text{comb}}$  to denote properties of the combined configuration, subscript  $\square_{\text{dev}}$  for properties of the measurement device only (assumed known in this section), and  $\square_{\text{obj}}$  for the object-under-test whose properties we ultimately desire. The Centres of Gravity (CoGs) and the inertia tensors of these 3 configurations are denoted  $\mathbf{x}_{\square}$  and  $(I_{ij})_{\square}$ , respectively, and are all expressed in IMU body coordinates  $B$ . Additionally, we introduce distances  $\mathbf{r} \triangleq \mathbf{x}_{\text{comb}} - \mathbf{x}_{\text{obj}}$  and  $\mathbf{s} \triangleq \mathbf{x}_{\text{comb}} - \mathbf{x}_{\text{dev}}$ . Refer again to Figure 2 for a visual representation.

Using these definitions and the general form of the parallel axis theorem [8], the measured inertia is

$$(I_{ij})_{\text{comb}} = (I_{ij})_{\text{obj}} + m_{\text{obj}} \left( |\mathbf{r}|^2 \delta_{ij} - r_i r_j \right) + (I_{ij})_{\text{dev}} + m_{\text{dev}} \left( |\mathbf{s}|^2 \delta_{ij} - s_i s_j \right). \quad (15)$$

where  $\delta_{ij}$  is again the Kronecker delta. Solving this yields

$$(I_{ij})_{\text{obj}} = (I_{ij})_{\text{comb}} - m_{\text{obj}} \left( |\mathbf{r}|^2 \delta_{ij} - r_i r_j \right) - (I_{ij})_{\text{dev}} - m_{\text{dev}} \left( |\mathbf{s}|^2 \delta_{ij} - s_i s_j \right). \quad (16)$$

As a reminder, we assume the properties of the measurement device  $\square_{\text{dev}}$  are known.  $(I_{ij})_{\text{comb}}$  is known from applying the procedure in the previous section and the masses can be determined with a scale. However,  $\mathbf{r}$  and  $\mathbf{s}$  require knowledge of the location of the Centre of Gravities (CoGs) with respect to the IMU.

For  $\mathbf{x}_{\text{obj}}$ , we can write

$$\mathbf{x}_{\text{obj}} = \frac{m_{\text{comb}}}{m_{\text{obj}}} \mathbf{x}_{\text{comb}} - \frac{m_{\text{dev}}}{m_{\text{obj}}} \mathbf{x}_{\text{dev}}, \quad (17)$$

and using  $m_{\text{comb}} = m_{\text{dev}} + m_{\text{obj}}$  we can express  $\mathbf{r}$  as

$$\mathbf{r} = \mathbf{x}_{\text{comb}} + \frac{m_{\text{dev}}}{m_{\text{obj}}} \mathbf{x}_{\text{dev}} - \frac{m_{\text{comb}}}{m_{\text{obj}}} \mathbf{x}_{\text{comb}} \quad (18)$$

$$= \frac{m_{\text{dev}}}{m_{\text{obj}}} (\mathbf{x}_{\text{dev}} - \mathbf{x}_{\text{comb}}). \quad (19)$$

The crux is now determining  $\mathbf{x}_{\text{comb}}$ , which can be obtained by applying the method shown in [9] to the same tumbling data used in the previous section. The principle can be summarized as follows: in the assumed freefall, the accelerometer sensors in the IMU measure the centripetal and tangential acceleration due to the rotation of the body. Because these angular velocities are known and their derivatives can be estimated, this enables finding the offset between the IMU and the centre of gravity within sub-centimetre accuracy.

### D. Calibrating reaction wheel inertia and device inertia

The previous sections derived the estimation assuming reaction wheel inertia  $I_R$  and measurement device CoG  $\mathbf{x}_{\text{dev}}$  and inertia  $(I_{ij})_{\text{dev}}$  are known. We now propose a calibration procedure that works by applying the method in the previous sections to throw data of 2 configurations with known attached object inertias  $(I_{ij})_{\text{obj}}$ .

Similarly to how the left-hand side of Equation 6 could be decomposed into  $\zeta_i \boldsymbol{\theta}$  in Equation 8, the right-hand side can be expressed as  $\eta_i \boldsymbol{\varphi}$ , where  $\boldsymbol{\varphi}$  contains the inertia elements of the spinning reaction wheel.  $\eta_i$  is a similar cross-product evaluation as shown in Equation 9. This gives

$$\zeta_i \boldsymbol{\theta} = \eta_i \boldsymbol{\varphi}, \quad (20)$$

where  $\boldsymbol{\theta}$  and  $\boldsymbol{\varphi}$  are linearly dependent and cannot be solved simultaneously. However, if  $\boldsymbol{\omega}_R = (0 \ 0 \ \omega_{R,z})^T$ , and  $I_{R,xz} = I_{R,yz} = 0$  from axial symmetry, then the right-hand side of Equation 6 collapses to  $-I_{R,zz} (\dot{\boldsymbol{\omega}}_R + \boldsymbol{\omega} \times \boldsymbol{\omega}_R)$ . This allows parametrising  $\boldsymbol{\varphi} = (0 \ 0 \ 0 \ 0 \ 0 \ I_{R,zz})^T$ .

We set  $I_{R,zz} = 1$ , and perform the data analysis procedure outlined in subsection II-B for throws of 2 known  $(I_{ij})_{\text{obj}}$  and  $m_{\text{obj}}$ . These analyses yield  $(\hat{I}_{ij})_{\text{comb}}$ , which needs to be scaled by the true  $I_{R,zz}$  (see Equation 20) to yield the true combined inertias

$$\begin{aligned} (I_{ij})_{\text{comb}}^1 &= I_{R,zz} \left( \hat{I}_{ij} \right)_{\text{comb}}^1 \\ (I_{ij})_{\text{comb}}^2 &= I_{R,zz} \left( \hat{I}_{ij} \right)_{\text{comb}}^2. \end{aligned} \quad (21)$$

Plugging this into 2 instances of Equation 15 gives 12 equations in 10 unknowns  $(I_{R,zz}, (I_{ij})_{\text{dev}}, \mathbf{x}_{\text{dev}})$ . Solving the system can be simplified greatly by choosing that one of the

throws be performed without any body attached, which we call the device-only configuration with  $(I_{ij})_{\text{obj}}^1 = 0$  and  $m_{\text{obj}}^1 = 0$ .

The second configuration is called the proof-body configuration with known and non-zero  $(I_{ij})_{\text{proof}} \triangleq (I_{ij})_{\text{obj}}^2$  and  $m_{\text{proof}} \triangleq m_{\text{obj}}^2$ . The 2 instances of Equation 15 collapse to

$$I_{R,zz} \left( \hat{I}_{ij} \right)_{\text{comb}}^1 = (I_{ij})_{\text{dev}} \quad (22)$$

$$I_{R,zz} \left( \hat{I}_{ij} \right)_{\text{comb}}^2 = (I_{ij})_{\text{proof}} + m_{\text{proof}} \left( |\mathbf{r}|^2 \delta_{ij} - r_i r_j \right) + (I_{ij})_{\text{dev}} + m_{\text{dev}} \left( |\mathbf{s}|^2 \delta_{ij} - s_i s_j \right), \quad (23)$$

which can be trivially reduced to 6 equations in 1 unknown ( $I_{R,zz}$ ) by substituting the first into the second:

$$I_{R,zz} \left( \left( \hat{I}_{ij} \right)_{\text{comb}}^2 - \left( \hat{I}_{ij} \right)_{\text{comb}}^1 \right) = (I_{ij})_{\text{proof}} + m_{\text{proof}} \left( |\mathbf{r}|^2 \delta_{ij} - r_i r_j \right) + m_{\text{dev}} \left( |\mathbf{s}|^2 \delta_{ij} - s_i s_j \right) \quad (24)$$

The right-hand-side is known and the left-hand-side is known up to the scalar  $I_{R,zz}$ . By transforming the two sides into vectors following Equation 7, we can finally write the least-square solution for  $I_{R,zz}$  as the orthogonal projection of the right-hand side onto the left-hand side:

$$I_{R,zz} = \frac{\boldsymbol{\theta}_{lhs}^T \boldsymbol{\theta}_{rhs}}{|\boldsymbol{\theta}_{lhs}|^2}. \quad (25)$$

To summarize, Figure 3 illustrates which properties are obtained from what data.

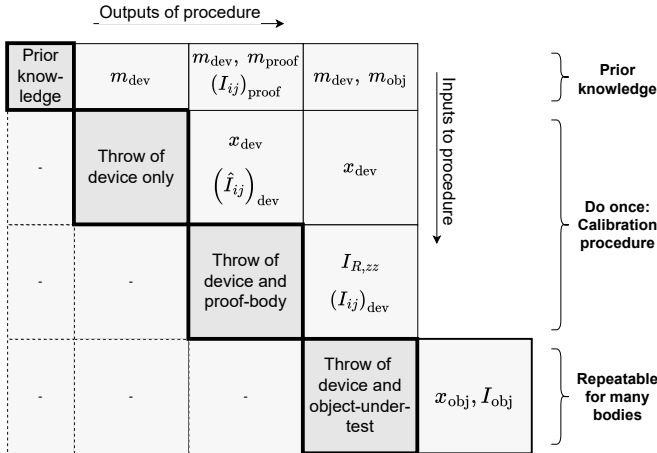


Figure 3: Visual depiction of the method. Subprocedures and their data on the diagonal, their required inputs vertically above, their output on the right.

### E. Error metrics

In order to distinguish between the error in the measured inertia magnitudes, and the error in the estimation of their rotational alignment, we propose two error metrics.

First, for the magnitudes: the principal moments of inertia are equal to the eigenvalues  $\lambda_x$ ,  $\lambda_y$  and  $\lambda_z$  of  $I_{\text{obj}}$ . Consequently, we define the relative inertial magnitude error as

$$\varepsilon = \frac{1}{|\boldsymbol{\theta}|} \sqrt{(\Delta\lambda_x)^2 + (\Delta\lambda_y)^2 + (\Delta\lambda_z)^2}, \quad (26)$$

where  $\Delta\lambda_i$  is equal to the error between the true principal inertia and the estimated principal inertia  $\lambda_i = (I_{ii})_p$ .

The spatial transformation from the matrix representation of  $I_{\text{obj}}$  to the diagonalised representation is a rotation, which can be found using the singular value decomposition (SVD) of  $I = U\Sigma V^T$ . We define the alignment error  $\psi$  as the geodesic distance between the ground truth  $\tilde{U}$  and the estimated  $U$ :

$$\psi = \arccos \frac{\text{Tr}(\tilde{U}^T U) - 1}{2}. \quad (27)$$

## III. EXPERIMENTAL VERIFICATION AND VALIDATION

In the previous section, we developed a method to estimate the inertia tensor of a rigid body using measurements of its rotational rates, linear specific forces and the speed of an attached reaction wheel. This section describes simulations and experiments performed to validate the procedure.

### A. Test Device

We collected the required data using a consumer-grade multirotor flight controller with onboard MEMS-IMU. The reaction wheel is actuated using a brushless DC motor, controlled by an Electronic Speed Controller (ESC) with motor rotation speed feedback. The device is powered using a 2S LiPo battery, weighs 100 g, and is pictured in Figure 4a.

The flight controller runs “INDIfight”<sup>3</sup>, a research-focussed fork of the high-performance flight control firmware “Betaflight”. The relevant modifications in this fork include the capability to detect throws based on acceleration and rate, and subsequently sending a programmable profile of motor commands to the ESC. The sampling and logging frequency was set to 4 kHz.

### B. Proof and validation bodies

The proof body required for the calibration procedure was chosen to be a cuboid of homogenous aluminium (not shown), machined to 70×60×30 mm. This is ideal for calibration, since its mass moments of inertia are accurately determined from geometry and mass, and significantly larger than those of the test device.

To demonstrate that the method is accurate for a versatile range of inertial properties, a grid-frame was 3D printed with pre-shaped holes for steel cuboids (shown in Figure 4b). This allows for a large number of configurations of weights, providing a large number of possible inertia tensors. Also for this body, we can accurately calculate its ground-truth inertia from the geometry and mass of a given configuration. This was necessary, since other experimental methods for measuring the moments of inertia either have been shown to have errors in the range of 3% [10] (pendulum method), require expensive machinery [11] or specific attachment points complicating construction [2].

<sup>3</sup>[https://github.com/tudelft/indiflight/tree/inertia\\_by\\_throwing](https://github.com/tudelft/indiflight/tree/inertia_by_throwing)

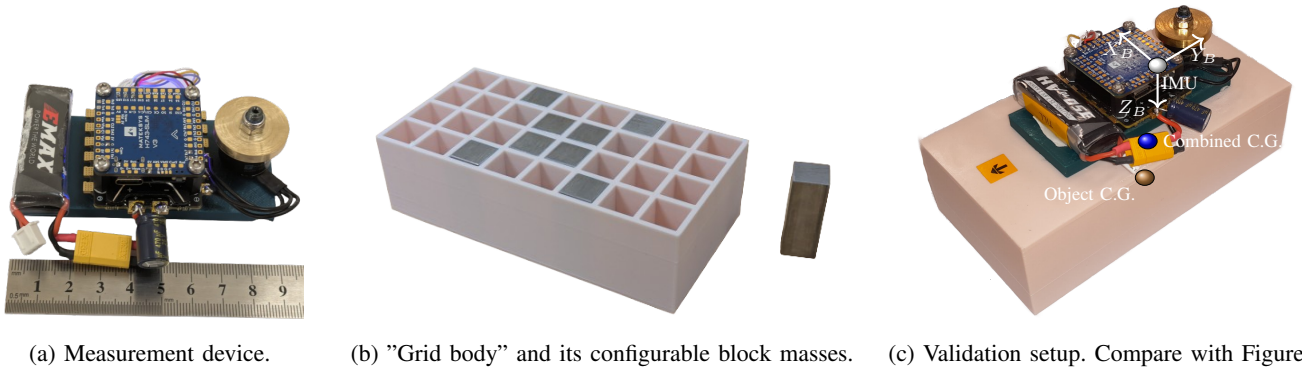


Figure 4: Overview of the experimental hardware.

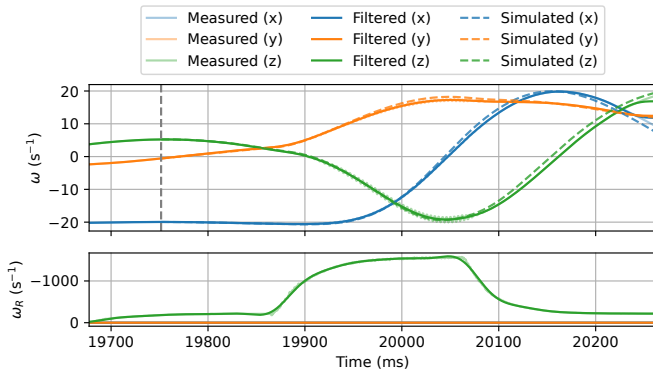


Figure 5: Simulation of the angular velocities, based on an initial condition at the dashed line, and the filtered flywheel rotation compared to measured and filtered angular velocities.

### C. Experimental procedure

We performed the calibration procedure from subsection II-D by combining data from multiple device-only and device + proof-body throws. With the resulting  $\mathbf{x}_{\text{dev}}$ ,  $(I_{ij})_{\text{dev}}$ , and reaction wheel  $I_{R,zz}$ , 4 different configurations of the grid body were thrown 10 or more times each. The method from subsection II-B and subsection II-C was run on the data of each throw *individually*, and then the errors were aggregated.

The arrangement and coordinate system used in the validation tests is shown in Figure 4c. The control signal sent to the reaction wheel motor is a pulse, as shown in the lower part of Figure 5.

### D. Additional verification and validation

To verify whether the method converges on a correct representation of the inertia tensor, forward integration simulations were performed and run through the algorithm presented to assess convergence to the assumed moments of inertia. There, the bottleneck to accuracy was found to be the numerical differentiation required for computing the angular acceleration. The algorithm otherwise converges to arbitrary accuracy, limited by the time step used for the numerical integration.

To demonstrate the validity of Equation 6, several simulations were performed, based on a single data point in the

falling phase, and the measured inertia tensor. For this, the measured reaction wheel angular rotation was filtered and then used to evaluate the right-hand side. A forward Euler integration scheme was then used to evaluate how well the measured inertia tensor produces the same rotation, given the same (filtered) input. One such simulation can be seen in Figure 5, where the dashed vertical line shows the initial condition.

## IV. RESULTS

Table I shows the aggregated experiment results with different configurations of the grid body. The inertia of the device and the reaction wheel have been calibrated from throws with and without the aluminium proof block attached.


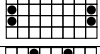
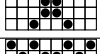
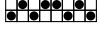
In the average case, the errors after processing data from single throws are below 3% of the magnitude of the true moments of inertia, and below  $4^\circ$  for the alignment of the principal axis system. For any configuration the maximum observed error from single throw data is 6.6%, and  $5.5^\circ$ , which both occur at configuration A.

The computation of the location of the CoG of the object (not the combination object + device!) from single throw data is also shown in the table. It was repeatable up to a standard deviation of below 0.5 mm; this worst-case also occurs at configuration A. However, no ground truth is available for  $x$  and  $y$  of this quantity, as the precise location of the measurement device on the grid body has not been recorded. The height of the IMU with respect to the body was recorded however, and so the  $z$ -distance between the calculated CoG and IMU is shown in the CoGz column of Table I. It is within 0.6 mm of the estimated  $z$ -coordinate, worst case.

## V. DISCUSSION

The results show some variation in the inertia tensor, which could be due to various causes. First, we noticed some sensitivity to low-pass filter settings. Putting the filter cut-off frequency too low dampened relevant frequencies from the data, leading to much higher errors. Putting the cut-off frequency too high also has a detrimental effect, since the increased noise reduces the accuracy of the numerical differentiation significantly. Low-frequency vibrations from violating the rigid-body assumption (e.g. from loose wires),

Table I: Aggregated experiment results. Percentage inertia component errors  $\varepsilon$  and alignment error  $\Psi$  are shown for the different configurations, as well as CoG estimates (value along  $X_B$ ,  $Y_B$  unvalidated, as no ground truth exists).

Ground truth from geometry				Our algorithms, run on data of single throws						
Configuration	m [kg]	CoGz [mm]	diagI [kg mm <sup>2</sup> ]	N	mean( $\varepsilon$ )	max( $\varepsilon$ )	mean( $\Psi$ )	max( $\Psi$ )	mean( $\hat{x}$ ) [mm]	stddev( $\hat{x}$ ) [mm]
E: 	0.178	43.4	[368 123 431]	10	1.6%	2.3%	2.1°	2.4°	[10.7 1.8 43.1]	[0.2 0.23 0.24]
A: 	0.459	45.3	[1525 190 1577]	11	1.7%	6.6%	3.5°	5.5°	[10.7 2.3 45.9]	[0.18 0.46 0.49]
B: 	0.739	45.8	[682 437 906]	12	1.8%	4.3%	2.1°	2.2°	[10.7 1.4 45.6]	[0.14 0.06 0.09]
C: 	1.300	46.1	[2448 750 2835]	12	2.5%	4.1%	1.6°	1.9°	[10.5 1.7 46.1]	[0.06 0.28 0.19]

can have detrimental effects on the accuracy and must be avoided.

Another consideration is that the reaction wheel inertia should be sufficiently large in order to generate enough torque. A small reaction wheel inertia leads to a low signal-to-noise ratio, which reduces the accuracy. At the same time, when the object has low inertia and the reaction wheel has high inertia, its speed must be limited to prevent exceeding the sensing limits of the gyroscope. Vibrations originating from an imbalanced reaction wheel then lead to noise, can saturate the accelerometer, and reduce accuracy.

Further, it is important to throw the device with enough spin around the unstable axis of rigid body rotation. Bodies that have no intermediate principal axis form a special case, demonstrated by configuration A. In these cases, the addition of the measurement device can be used to create a combined body which does have an intermediate principal axis, and the method still works. Table I does show that the accuracy of the estimate suffers when two principal inertias are close in magnitude. If the addition of the measurement device yields insufficient inertial change, a weight can be added to the measurement device (before calibration), to amend the combined inertia such that there is a sufficiently unstable axis.

In addition, the presented model does not account for the air resistance acting on the rotating body. Therefore, the method works best on densely packed bodies that are ideally roughly spherical. This limitation is not easily quantified and therefore left qualitative.

The accuracy of the estimate for the centre of gravity was not accurately determined in all directions. However, as the standard deviation is small and the error in one axis has been shown to be small, this give some indication of the accuracy one can expect.

## VI. CONCLUSIONS

We have shown a method to estimate Centre of Gravity (CoG) and mass moments of inertia of a rigid body from data recorded on a small attached measurement device during a manual throw. The device comprises a 3-axis gyroscope and accelerometer, as well as a small reaction wheel. A dynamical model of the system and data from free-spinning can be used to fit the inertial properties.

Calibration of the device and reaction wheel inertia was effectively achieved from throws of the device with and without an attached body of known mass properties. Then, the device

can be attached to other rigid bodies and the corresponding inertia matrix and CoG locations can be estimated, requiring only the mass of the body to be known. The mean errors in the magnitude of the principal inertias are around 2% from a single throw. The directions of the principal axes can be computed on average within about 2.5°.

If vertical spinning throws are convenient, and aerodynamic effects are not a factor, then the accuracy is comparable to that expected of pendulum methods, but requires less setup and directly provides CoG and principal axis directions as outputs.

## ACKNOWLEDGEMENT

ChatGPT provided assistance in writing the analysis code.

## REFERENCES

- [1] C. Schedlinski and M. Link, "A Survey of Current Inertia Parameter Identification Methods," *Mechanical Systems and Signal Processing*, vol. 15, no. 1, pp. 189–211, 2001.
- [2] L. Tang and W. B. Shangquan, "An improved pendulum method for the determination of the center of gravity and inertia tensor for irregular-shaped bodies," *Measurement*, vol. 44, no. 10, pp. 1849–1859, 2011.
- [3] M. Jardin and E. Mueller, "Optimized Measurements of UAV Mass Moment of Inertia with a Bifilar Pendulum," in *AIAA Guidance, Navigation and Control Conference and Exhibit*. Hilton Head, South Carolina: American Institute of Aeronautics and Astronautics, 2007.
- [4] T. Setati, N. Botha, and J. M. Roux, "Experimental approach to calculate the moments of inertia of a hexacopter unmanned aerial vehicle," in *Annual International RAPDASA Conference*, vol. 370, 2022, pp. 1–11.
- [5] K. Fukami and S.-I. Higashino, "Experimental Method for Determination of Virtual Inertia Matrix Using Multivariate Regression Analysis," *Sensors and Materials*, vol. 31, no. 12, p. 4247, 2019.
- [6] K. Lehmkuhler, K. Wong, and D. Verstraete, "Methods for accurate measurements of small fixed wing UAV inertial properties," *The Aeronautical Journal*, vol. 120, no. 1233, pp. 1785–1811, 2016.
- [7] Herbert Goldstein, Charles P. Poole, and John L. Safko, *Classical Mechanics*, 3rd ed. Reading, Mass., USA: Addison-Wesley, 2002.
- [8] A. R. Abdulghany, "Generalization of parallel axis theorem for rotational inertia," *American Journal of Physics*, vol. 85, no. 10, pp. 791–795, 2017.
- [9] T. M. Blaha, E. J. Smeur, B. D. Remes, and C. C. de Visser, "Flying a quadrotor with unknown actuators and sensor configuration," in *International Micro Air Vehicle Conference and Competition*, T. Richardson, Ed., Bristol, United Kingdom, 2024, pp. 193–199.
- [10] J. J. Dowling, J. L. Durkin, and D. M. Andrews, "The uncertainty of the pendulum method for the determination of the moment of inertia," *Medical Engineering & Physics*, vol. 28, no. 8, pp. 837–841, 2006.
- [11] Z. C. Hou, Y. n. Lu, Y. x. Lao, and D. Liu, "A new trifilar pendulum approach to identify all inertia parameters of a rigid body or assembly," *Mechanism and Machine Theory*, vol. 44, no. 6, pp. 1270–1280, 2009.